nature medicine

PDK1 decreases TACE-mediated α-secretase activity and promotes disease progression in prion and Alzheimer's diseases

Mathéa Pietri[1,2], Caroline Dakowski[1,2], Samia Hannaoui[3–5], Aurélie Alleaume-Butaux[1,2], Julia Hernandez-Rapp[1,2,6], Audrey Ragagnin[7], Sophie Mouillet-Richard[1,2], Stéphane Haik[3–5], Yannick Bailly[7], Jean-Michel Peyrin[8], Jean-Marie Launay[9,10], Odile Kellermann[1,2] & Benoit Schneider[1,2]

α-secretase–mediated cleavage of amyloid precursor protein (APP) precludes formation of neurotoxic amyloid-β (Aβ) peptides, and α-cleavage of cellular prion protein (PrP^C) prevents its conversion into misfolded, pathogenic prions (PrP^{Sc}). The mechanisms leading to decreased α-secretase activity in Alzheimer's and prion disease remain unclear. Here, we find that tumor necrosis factor-α–converting enzyme (TACE)-mediated α-secretase activity is impaired at the surface of neurons infected with PrP^{Sc} or isolated from APP-transgenic mice with amyloid pathology. 3-phosphoinositide–dependent kinase-1 (PDK1) activity is increased in neurons infected with prions or affected by Aβ deposition and in the brains of individuals with Alzheimer's disease. PDK1 induces phosphorylation and caveolin-1–mediated internalization of TACE. This dysregulation of TACE increases PrP^{Sc} and Aβ accumulation and reduces shedding of TNF-α receptor type 1 (TNFR1). Inhibition of PDK1 promotes localization of TACE to the plasma membrane, restores TACE-dependent α-secretase activity and cleavage of APP, PrP^C and TNFR1, and attenuates PrP^{Sc}- and Aβ-induced neurotoxicity. In mice, inhibition or siRNA-mediated silencing of PDK1 extends survival and reduces motor impairment following PrP^{Sc} infection and in APP-transgenic mice reduces Alzheimer's disease-like pathology and memory impairment.

Prion and Alzheimer's disease are neurodegenerative disorders characterized by the accumulation of plaques containing misfolded PrP^{Sc} and Aβ, respectively[1,2]. Neurotoxic and aggregation-prone Aβ peptides ($Aβ_{40}$ and $Aβ_{42}$) are generated by cleavage of APP by β- and γ-secretase[3]. In contrast, the α-secretase–mediated cleavage of APP between residues 687 and 688 within its Aβ domain releases the soluble neuroprotective fragment sAPPα and precludes formation and deposition of $Aβ_{40}$ and $Aβ_{42}$ (refs. 4,5). Regarding prions, conversion of glycosylphosphatidylinositol (GPI)-anchored PrP^C into PrP^{Sc} causes prion disease. α-secretase–mediated cleavage of PrP^C between residues 111 and 112 generates an N-terminally truncated form of PrP^C that cannot be converted into PrP^{Sc} and exerts a dominant-negative effect on PrP^{Sc} replication[6].

α-secretases belong to the a disintegrin and metalloproteinase (ADAM) family involved in ectodomain shedding of growth factors, cytokines, receptors and adhesion molecules[7]. Tumor necrosis factor-α (TNF-α)-converting enzyme (TACE, or ADAM17), which is primarily known for its role in mediating the shedding of cell surface–bound TNF-α and TNF-α receptors[8], contributes to constitutive and/or stimulated α-secretase–mediated cleavage of both PrP^C and APP[3,9,10]. In individuals with Alzheimer's disease, low amounts of sAPPα in the cerebrospinal fluid (CSF) suggest that TACE-dependent α-secretase activity is reduced[11]. In prion diseases, reduced TACE-mediated α-secretase cleavage of PrP^C is thought to occur during the course of the illness, as shown by the progressive decrease in N-terminally truncated PrP^C in the brain of infected mice[6,12].

The sheddase activity of TACE depends on its localization at the plasma membrane[7,8], but the precise mechanisms governing TACE trafficking and activity remain poorly understood. Interaction of TACE with rhomboids[13] or post-translational modifications of TACE by glycosylation, phosphorylation or both[8] promote its localization to lipid rafts at the plasma membrane[14]. Reactive oxygen species have also been shown to stimulate TACE activity[15,16]. However, the direct mechanisms underlying reduced TACE-mediated α-secretase activity in prion and Alzheimer's disease remain unclear.

Here we show in both PrP^{Sc}-infected and Alzheimer's disease neurons that activation of 3-phosphoinositide–dependent kinase-1 (PDK1) reduces cell surface TACE-mediated α-secretase activity by triggering

[1]Institut National de la Santé et de la Recherche Médicale (INSERM), UMR-S 747, Paris, France. [2]Université Paris Descartes, Sorbonne Paris Cité, UMR-S 747, Paris, France. [3]Université Pierre et Marie Curie-Paris 6, Centre de Recherche de l'Institut du Cerveau et de la Moelle épinière, UMR-S 975, Equipe "Alzheimer's and Prion diseases," Paris, France. [4]INSERM, UMR-S 975, Paris, France. [5]Centre National de la Recherche Scientifique (CNRS) UMR 7225, Paris, France. [6]Université Paris Sud 11, ED419 Biosigne, Orsay, France. [7]Cytologie et Cytopathologie Neuronales, Institut des Neurosciences Cellulaires & Intégratives, CNRS UPR 3212, Strasbourg, France. [8]Neurobiologie des Processus Adaptatifs, CNRS UMR 7102, Université Pierre et Marie Curie–Paris 6, Paris, France. [9]Assistance Publique–Hôpitaux de Paris, Service de Biochimie, INSERM UMR-S 942, Hôpital Lariboisière, Paris, France. [10]Pharma Research Department, Hoffmann La Roche, Basel, Switzerland. Correspondence should be addressed to B.S. (benoit.schneider@parisdescartes.fr) or J.-M.L. (jean-marie.launay@lrb.aphp.fr).

Received 2 May; accepted 16 July; published online 18 August 2013; doi:10.1038/nm.3302

internalization of TACE. We also provide evidence that PDK1 inhibition attenuates prion and Alzheimer's disease progression.

RESULTS

Prion infection impairs TACE-dependent TNFR1 shedding

To investigate whether prion infection modulates TACE activity, we used 1C11 mouse neuroectodermal stem cells, serotonergic 1C11$^{5\text{-HT}}$ neural cells, primary cultures of mouse cerebellar granule neurons (CGNs) and brain samples from C57BL/6J mice infected with mouse-adapted prions derived from a human familial prion disease (Fukuoka-1, Fk), scrapie (22L) or bovine spongiform encephalopathy (6PB1)[17–19] (**Supplementary Fig. 1**). Using TNFR1 shedding as a readout of TACE activity[7], we found that prion infection triggered an approximately three- to four-fold increase in the amount of trimeric TNFR1 (ref. 20) at the cell surface (**Fig. 1a**). This increase in cell surface TNFR1 staining was associated with a 90% reduction in the concentration of soluble monomeric TNFR1 (sTNFR1) in the culture medium of infected cells as compared to uninfected cells (**Fig. 1b**). This increase in TNFR1 at the cell surface rendered prion-infected cells highly vulnerable to soluble TNF-α (sTNF-α)-associated toxicity. The doses of sTNF-α inducing 50% cell death ($LD_{50}^{sTNF\text{-}\alpha}$) of infected 1C11 and 1C11$^{5\text{-HT}}$ neural cells or causing 50% early neuronal dysfunction, that is, dendritic fragmentation, in infected CGNs were reduced by approximately 50–97% as compared to the doses achieving similar effects in their uninfected counterparts (**Fig. 1c** and **Supplementary Table 1**). The increased sensitivity of infected cells to sTNF-α was associated with increased sTNF-α–mediated caspase-3 activation (**Supplementary Fig. 2**), a downstream effector of TNFR1 signaling.

TNFR1 staining was increased in the cerebellar cortex and deep cerebellar nuclei of prion-infected mice killed just before the symptomatic phase as compared to mock-inoculated (sham) mice (**Supplementary Fig. 3**). The concentration of sTNFR1 in the CSF of 22L-infected mice (11.9 ± 2.4 pg ml^{-1}, n = 10) was reduced by approximately 60% (P < 0.005) as compared to uninfected mice (27.5 ± 5.1 pg ml^{-1}, n = 10). Taken together, these results suggest that prion infection reduces TACE-mediated shedding of TNFR1.

Prion infection promotes TACE internalization

Whereas TACE was normally present at the cell surface of uninfected cells, it was almost undetectable at the plasma membrane of prion-infected cells and found intracellularly (**Supplementary Fig. 4a**,**e**). We next analyzed TACE localization by detergent-free sucrose gradient membrane fractionation of cell extracts followed by western blotting or TACE immunoprecipitation of biotinylated plasma membrane proteins. We showed that TACE co-distributed with focal adhesion kinase (FAK) at the plasma membrane of uninfected 1C11$^{5\text{-HT}}$ cells (**Supplementary Fig. 4a–c**,**e**), whereas it co-distributed with caveolin-1 (Cav-1) in Fk-infected 1C11$^{5\text{-HT}}$ cells (**Supplementary Fig. 4b**). Duolink proximity ligation analysis, which detects two proteins located within a radius of <40 nm of each other, suggests that internalized TACE colocalizes with Cav-1 in Fk-infected 1C11$^{5\text{-HT}}$ cells (**Fig. 2a**). Immunogold labeling revealed that TACE was associated with Cav-1–enriched microvesicles in infected neurons (**Fig. 2b**). Thus, prion infection promotes internalization of TACE through mechanisms that probably involve Cav-1–enriched microvesicles. Accordingly, bombardment of Fk-infected 1C11$^{5\text{-HT}}$ cells with tungsten microprojectiles coated with Cav-1–specific antibodies[21] increased TACE trafficking to the plasma membrane (**Supplementary Fig. 4b**).

Phosphorylation of the C-terminal cytoplasmic tail of TACE alters TACE trafficking and internalization[7,8,22]. The TACE C-terminal domain contains at least four putative phosphorylation sites, including the single known phosphorylatable residue, Thr735 (refs. 7,8). Using two-dimensional gel electrophoresis (**Supplementary Fig. 4d**) and immunoprecipitation (**Fig. 2c**), we found that phosphorylation of TACE at Thr735 was increased in Fk-infected 1C11 and 1C11$^{5\text{-HT}}$ cells as compared to uninfected cells.

Prion infection–mediated PDK1 activation reduces TACE activity

The Src kinase–phosphatidylinositol 3-kinase (PI3K)-PDK1 signaling cascade and the

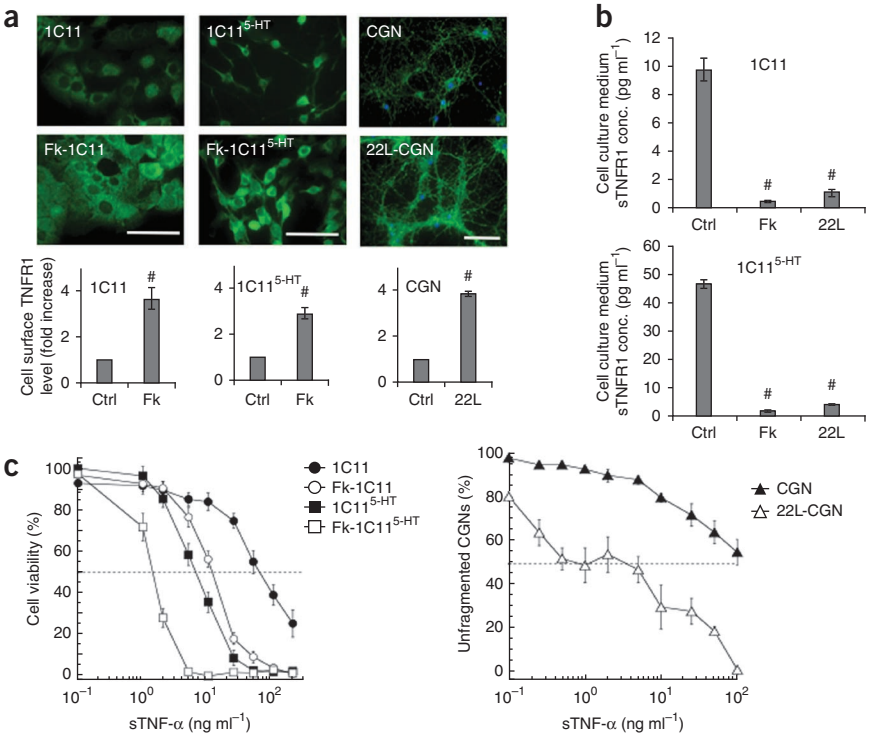

Figure 1 Prion infection reduces TNFR1 shedding and increases cellular sensitivity to sTNF-α toxicity. (**a**) Immunofluorescent labeling of TNFR1 at the surface of Fk-infected 1C11 precursors, 1C11$^{5\text{-HT}}$ neural cells and 22L-infected CGNs as compared to their uninfected counterparts (Ctrl). Scale bars, 50 μm. (**b**) Concentration of sTNFR1 in the culture medium of Fk- and 22L-infected 1C11 and 1C11$^{5\text{-HT}}$ cells as compared to uninfected cells. (**c**) Left, viability of Fk-infected 1C11 and 1C11$^{5\text{-HT}}$ cells after exposure to increasing concentrations of sTNF-α for 72 h as compared to uninfected cells. Right, dendritic fragmentation in 22L-infected CGNs after exposure to increasing sTNF-α concentrations for 72 h as compared to uninfected CGNs. $LD_{50}^{sTNF\text{-}\alpha}$ values are indicated in **Supplementary Table 1**. Quantitative data are shown as the mean ± s.e.m. from three experiments performed in triplicate; #P < 0.005 versus uninfected cells.

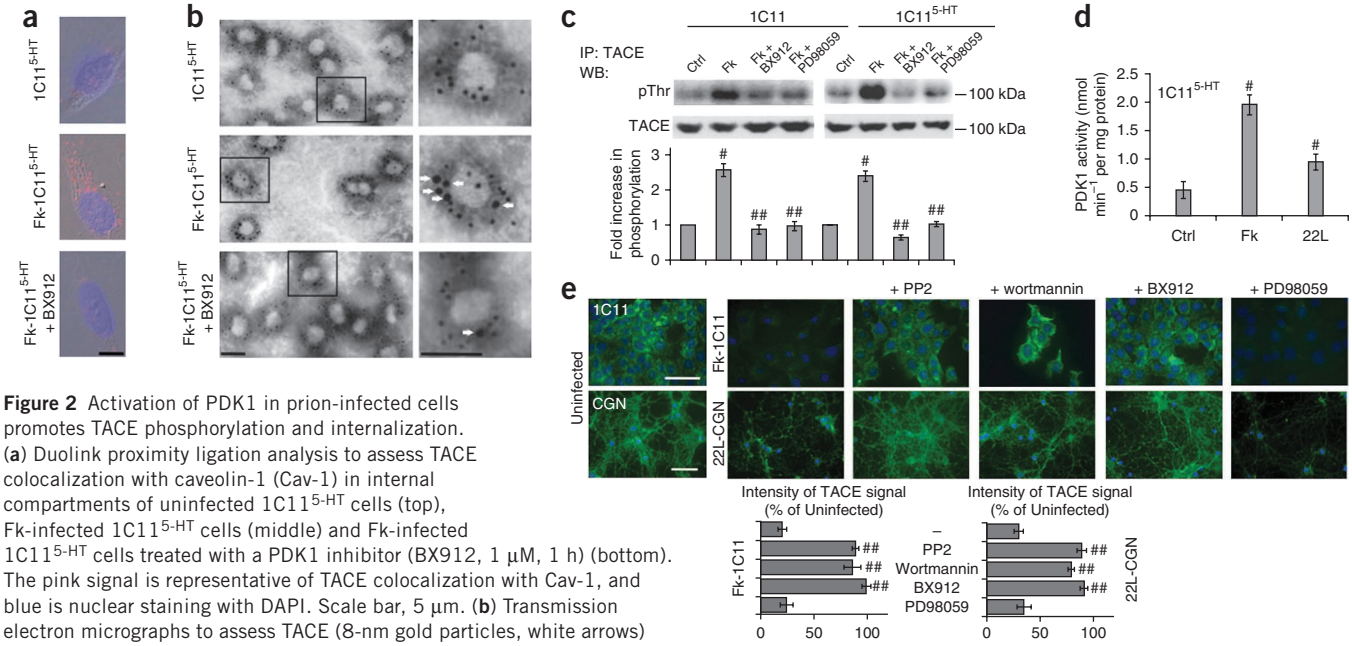

Figure 2 Activation of PDK1 in prion-infected cells promotes TACE phosphorylation and internalization. (**a**) Duolink proximity ligation analysis to assess TACE colocalization with caveolin-1 (Cav-1) in internal compartments of uninfected 1C11$^{5\text{-HT}}$ cells (top), Fk-infected 1C11$^{5\text{-HT}}$ cells (middle) and Fk-infected 1C11$^{5\text{-HT}}$ cells treated with a PDK1 inhibitor (BX912, 1 μM, 1 h) (bottom). The pink signal is representative of TACE colocalization with Cav-1, and blue is nuclear staining with DAPI. Scale bar, 5 μm. (**b**) Transmission electron micrographs to assess TACE (8-nm gold particles, white arrows) association with Cav-1–enriched vesicles (labeled by 5-nm gold particles) in uninfected 1C11$^{5\text{-HT}}$ cells (top), Fk-infected 1C11$^{5\text{-HT}}$ cells (middle) and Fk-infected 1C11$^{5\text{-HT}}$ cells exposed to BX912 (1 μM, 1 h) (bottom). Scale bars, 100 nm. (**c**) Immunoprecipitation of TACE and immunoblotting for phosphorylation level on threonine residues (pThr) using a pan–pThr antibody in Fk-infected 1C11 and 1C11$^{5\text{-HT}}$ cells treated or not with BX912 (1 μM, 1 h) or PD98059 (5 μM, 1 h) versus uninfected cells (Ctrl). IP, immunoprecipitation; WB, western blot. (**d**) PDK1 activity in 22L- and Fk-infected and uninfected (Ctrl) 1C11$^{5\text{-HT}}$ neural cells. (**e**) Immunofluorescent labeling of TACE at the surface of Fk-infected 1C11 cells and 22L-infected CGNs treated or not with inhibitors of Src kinases (PP2, 1 μM), PI3K (wortmannin, 1 μM), PDK1 (BX912, 1 μM) or ERK1/2 (PD98059, 5 μM) for 1 h versus uninfected cells. Scale bars, 50 μm. All experiments were performed three times in triplicate. Values are the mean ± s.e.m. #$P < 0.005$ versus uninfected cells (Ctrl); ##$P < 0.005$ versus untreated infected cells.

protein kinase C–extracellular signal–regulated kinase 1/2 (ERK1/2) pathway are both involved in the phosphorylation of the cytoplasmic tail of TACE in TACE-transfected cells[8].

PDK1 activity was increased by approximately 100–300% in infected 1C11$^{5\text{-HT}}$ neural cells as compared to their uninfected counterparts (**Fig. 2d**). Inhibition of PDK1 with BX912 in Fk-infected

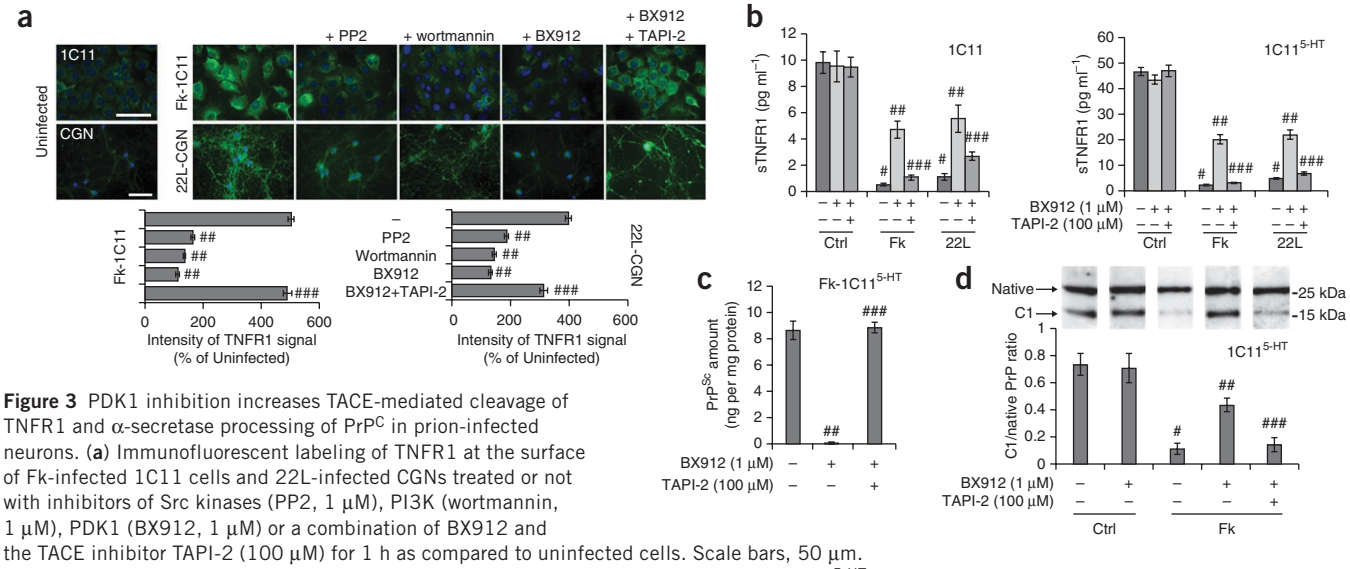

Figure 3 PDK1 inhibition increases TACE-mediated cleavage of TNFR1 and α-secretase processing of PrP^{C} in prion-infected neurons. (**a**) Immunofluorescent labeling of TNFR1 at the surface of Fk-infected 1C11 cells and 22L-infected CGNs treated or not with inhibitors of Src kinases (PP2, 1 μM), PI3K (wortmannin, 1 μM), PDK1 (BX912, 1 μM) or a combination of BX912 and the TACE inhibitor TAPI-2 (100 μM) for 1 h as compared to uninfected cells. Scale bars, 50 μm. (**b**) Concentration of sTNFR1 in the culture medium of Fk- and 22L-infected 1C11 and 1C11$^{5\text{-HT}}$ cells treated or not with BX912 (1 μM) or a combination of BX912 (1 μM) and TAPI-2 (100 μM) as compared to uninfected cells (Ctrl). (**c**) Amount of PrP^{Sc} in Fk-infected 1C11$^{5\text{-HT}}$ cells treated or not with BX912 (1 μM) or a combination of BX912 (1 μM) and TAPI-2 (100 μM) for 6 h, as assessed by ELISA. (**d**) Western blot analysis (top) of the C1 fragment of PrP (C1) and full-length PrP (native) in Fk-infected 1C11$^{5\text{-HT}}$ cells treated or not with BX912 (1 μM) or a combination of BX912 (1 μM) and TAPI-2 (100 μM) for 6 h versus uninfected cells (Ctrl) and the ratio (bottom) of C1/native full-length PrP. All experiments were performed three times in triplicate. Values are the mean ± s.e.m. #$P < 0.005$ versus uninfected cells (Ctrl); ##$P < 0.005$ versus untreated Fk- or 22L-infected cells. ###$P < 0.005$ versus BX912-treated Fk- or 22L-infected cells.

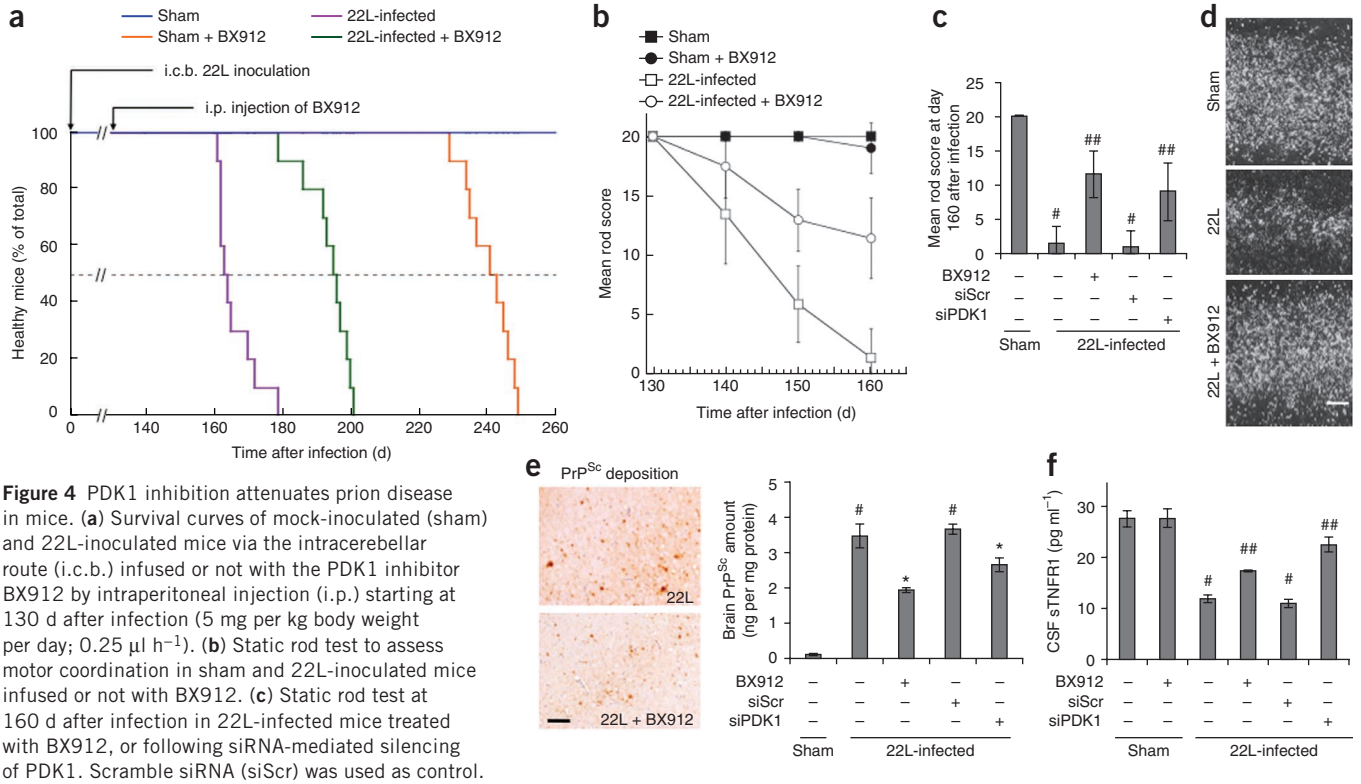

Figure 4 PDK1 inhibition attenuates prion disease in mice. (**a**) Survival curves of mock-inoculated (sham) and 22L-inoculated mice via the intracerebellar route (i.c.b.) infused or not with the PDK1 inhibitor BX912 by intraperitoneal injection (i.p.) starting at 130 d after infection (5 mg per kg body weight per day; 0.25 µl h^{-1}). (**b**) Static rod test to assess motor coordination in sham and 22L-inoculated mice infused or not with BX912. (**c**) Static rod test at 160 d after infection in 22L-infected mice treated with BX912, or following siRNA-mediated silencing of PDK1. Scramble siRNA (siScr) was used as control. (**d**) Nissl staining of viable PCNA-positive neurons in the internal granular layer of the cerebellum of sham mice (top), 22L-infected mice at 179 d after infection (middle) and 22L-infected mice at 201 d after infection infused with BX912 starting at 130 d (bottom). Scale bar, 300 µm. (**e**) Left, cerebellar immunoperoxidase staining to visualize PrP^{Sc} deposition in brains of 22L-infected mice infused or not with BX912. Scale bar, 100 µm. Right, postmortem quantification of proteinase K–resistant PrP^{Sc} in brains of 22L-infected mice treated with BX912 or following siRNA-mediated PDK1 silencing (siPDK1). SiScr was used as control. (**f**) Concentration of sTNFR1 in the CSF of 22L-infected mice infused with BX912 or treated with siPDK1 versus control mice (sham and siScr-treated 22L mice). Values are the mean ± s.e.m. #$P < 0.005$ versus sham mice; ##$P < 0.01$ versus 22L-infected mice; *$P < 0.005$ versus 22L-infected mice. $n = 10$ mice per group.

1C11 and $1C11^{5\text{-HT}}$ cells reversed prion-induced TACE phosphorylation (**Fig. 2c** and **Supplementary Fig. 4d**). Moreover, inhibition of Src kinases (PP2), PI3K (wortmannin) or PDK1 (BX912) promoted translocation of TACE back to the surface of infected cells (**Fig. 2e** and **Supplementary Fig. 4e**). The intensity of TACE immunoreactivity at the surface of inhibitor-treated infected cells was similar to that in uninfected cells (**Fig. 2e**). Cell surface biotinylation experiments at 4 °C further showed that BX912 treatment of Fk-infected $1C11^{5\text{-HT}}$ neural cells failed to promote trafficking of TACE to the plasma membrane (**Supplementary Fig. 4c**), whereas BX912 treatment at 37 °C induced displacement of TACE from Cav-1–enriched microvesicles (**Fig. 2a**,**b**) to FAK-positive membrane fractions (**Supplementary Fig. 4b**,**c**).

We recently reported that prion infection enhances ERK1/2 phosphorylation[23]. Here, we observed that ERK1/2 activation increased TACE phosphorylation at Thr735 in Fk-infected 1C11 and $1C11^{5\text{-HT}}$ cells (**Fig. 2c**). However, inhibition of ERK1/2 activity with PD98059 in these infected cells did not promote trafficking of TACE to the plasma membrane (**Fig. 2e** and **Supplementary Fig. 4e**). To assess whether phosphorylation of TACE at residue Thr735 is sufficient to promote trafficking of TACE between the plasma membrane and Cav-1–enriched microvesicles, we transfected uninfected $1C11^{5\text{-HT}}$ cells with a TACE mutant that mimics a constitutive phosphorylation (T735D) or dephosphorylation (T735A) state. Both mutated TACEs stayed at the plasma membrane of uninfected cells, suggesting phosphorylation at Thr735 may not be sufficient to promote TACE internalization (data not shown).

Exposure of Fk-infected 1C11 cells and 22L-infected CGNs to PP2, wortmannin or BX912 reduced the amount of TNFR1 at the plasma membrane as compared to untreated infected cells (**Fig. 3a**), which suggested that TACE activity at the cell surface had been recovered. In Fk- and 22L-infected 1C11 and $1C11^{5\text{-HT}}$ cells, PDK1 inhibition increased the concentration of sTNFR1 in the cell medium by 60% as compared to untreated infected cells (**Fig. 3b**). Bombardment of infected $1C11^{5\text{-HT}}$ cells with tungsten microprojectiles coated with Cav-1–specific antibodies also increased TNFR1 shedding as compared to untreated infected cells (**Supplementary Fig. 5a**). Recovery of TNFR1 shedding by BX912 depended on TACE, as inhibition of TACE by incubation of cells with TNF-α processing inhibitor-2 (TAPI-2) abrogated the effects of BX912 on shedding of TNFR1 from the cell surface (**Fig. 3a**) into the culture medium (**Fig. 3b**). The increase in TNFR1 shedding upon PDK1 inhibition also decreased sTNF-α–induced activation of caspase-3 in infected cells (**Supplementary Fig. 2**).

TACE-mediated α-secretase cleavage of PrP^{C} between residues 111 and 112 generates an N-terminally truncated (that is, membrane C1) fragment that cannot be converted into PrP^{Sc} (refs. 6,9). PDK1 inhibition with BX912 in Fk-infected $1C11^{5\text{-HT}}$ cells decreased the amount of PrP^{Sc}, which was reversed by inhibition of TACE with TAPI-2 (**Fig. 3c**). Bombardment of infected $1C11^{5\text{-HT}}$ cells with tungsten microprojectiles coated with Cav-1–specific antibodies also reduced the amount of PrP^{Sc} (**Supplementary Fig. 5b**). In Fk-infected $1C11^{5\text{-HT}}$ cells, the ratio between PrP C1 fragment

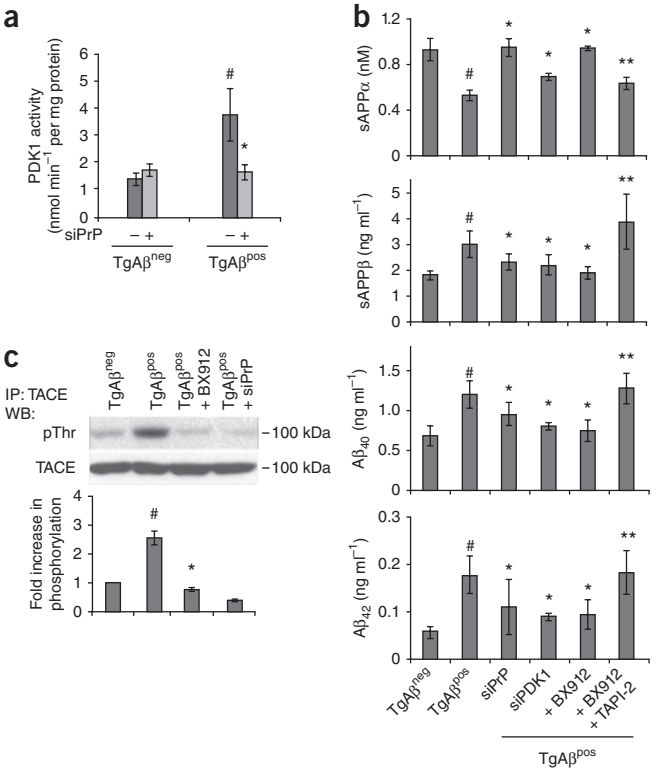

Figure 5 Increased PDK1 activity in hippocampal neurons from mice with Alzheimer's disease–like pathology impairs TACE activity. (**a**) PDK1 activity in primary hippocampal neurons derived from 275-day-old Tg2576 mice with Aβ plaque deposits ($TgA\beta^{pos}$, $n = 4$) and without Aβ deposits ($TgA\beta^{neg}$, $n = 5$) as well as in $TgA\beta^{pos}$ and $TgA\beta^{neg}$ neurons in which PrP^C expression was silenced with a siRNA against PrP (siPrP, $n = 4$). (**b**) Concentration of sAPPα, sAPPβ, $A\beta_{40}$ and $A\beta_{42}$ in the culture medium of $TgA\beta^{pos}$ neurons as compared to those of $TgA\beta^{neg}$ neurons, $TgA\beta^{pos}$ neurons silenced for PrP^C (siPrP) or PDK1 (siPDK1) expression, and $TgA\beta^{pos}$ neurons treated with BX912 (1 μM) combined or not with TAPI-2 (100 μM) for 1 h ($n = 4$ for each group). (**c**) Immunoprecipitation experiments to assess TACE threonine phosphorylation in $TgA\beta^{pos}$ and $TgA\beta^{neg}$ neurons. Impact of PDK1 inhibition with BX912 (1 μM, 1 h) or silencing of PrP (siPrP) on TACE threonine phosphorylation in $TgA\beta^{pos}$ neurons ($n = 3$ in triplicate) is also shown. Values are the mean ± s.e.m. $\#P < 0.05$ versus $TgA\beta^{neg}$ neurons; $*P < 0.05$ versus untreated $TgA\beta^{pos}$ neurons; $**P < 0.05$ versus $TgA\beta^{pos}$ neurons treated with BX912.

to full-length PrP (native) was reduced by approximately 85% as compared to that in uninfected cells (**Fig. 3d**). The C1/native ratio was increased by approximately 300% in BX912-treated Fk-1C11$^{5\text{-HT}}$ cells compared to untreated infected cells (**Fig. 3d**). This increase in α-secretase cleavage of PrP^C by BX912 depends on TACE, as inhibition of TACE with TAPI-2 counteracted the effects of BX912 on the C1/native PrP ratio (**Fig. 3d**).

PDK1 inhibition improves prion disease in mice

To examine whether increasing TACE-mediated α-secretase activity would attenuate prion disease in prion-infected mice, we chronically injected BX912 intraperitoneally (i.p.) starting 130 d after infection and before the onset of clinical signs (140 d). Inhibition of PDK1 with BX912 delayed mortality in 22L-infected mice as compared to untreated infected mice (193.8 ± 2.1 d versus 166.0 ± 1.8 d, $n = 10$, $P < 0.0001$, **Fig. 4a**). In control experiments, because of BX912's toxicity[24], mock-inoculated (sham) mice treated with BX912 died from 229 to 248 d (**Fig. 4a**). This mortality probably leads to an underestimation of the beneficial effect of PDK1 inhibition in infected mice. PDK1 inhibition also reduced prion infection–induced impairments in motor function (**Fig. 4b**). In 22L-infected mice, the mean static rod score dropped to 10 by 145 d, whereas in BX912-treated infected mice the mean static score did not drop below 10 until 160 d. In sham mice, motor coordination was unchanged by BX912 treatment (**Fig. 4b**). PDK1 siRNA–mediated silencing of PDK1 in the brain of 22L-infected mice also prevented prion-induced motor impairment (**Fig. 4c**). PDK1 inhibition with BX912 also attenuated prion-induced neuronal loss in the internal granular layer of the cerebellum, as assessed by staining of viable neurons (**Fig. 4d**). BX912 treatment or siRNA-mediated PDK1 silencing reduced the amount of PrP^{Sc} deposited in the brains of 22L-infected mice (**Fig. 4e**). Finally, BX912 treatment or PDK1 silencing partly, but significantly, increased TACE-mediated shedding of TNFR1, as indicated by an increased concentration of sTNFR1 in the CSF of infected mice (**Fig. 4f**).

Aβ accumulation in Alzheimer's neurons overactivates PDK1

In Alzheimer's disease, decreased TACE-mediated α-secretase cleavage of APP is believed to contribute to the accumulation of Aβ peptides and to the progression of the disease[11,25]. Recent data suggest that PrP^C is involved in Aβ peptide neurotoxicity[26,27]. Our identification of a PDK1-dependent mechanism controlling the trafficking and α-secretase activity of TACE in prion-infected cells prompted us to examine whether the accumulation of Aβ peptide would increase PDK1 activity and whether this occurs through a PrP^C-dependent mechanism. Increased PDK1 activity would, in turn, affect TACE-dependent cleavage of TNFR1 and APP.

The Tg2576 APP (Swedish mutation K670N/M671L) mouse model of Alzheimer's disease[28] develops amyloid pathology and Aβ plaque deposition in the brain as early as 8 months of age[29]. Tg2576 mice with ($TgA\beta^{pos}$) or without ($TgA\beta^{neg}$) amyloid plaque deposits were identified by positron emission tomography (PET) imaging after Pittsburgh compound B injection[30]. PDK1 activity was increased by approximately 150% in primary cultures of hippocampal neurons derived from 275-day-old $TgA\beta^{pos}$ mice as compared to $TgA\beta^{neg}$ mice (**Fig. 5a**). siRNA-mediated silencing of PrP^C (siPrP) in $TgA\beta^{pos}$ cultured hippocampal neurons reversed the increase in PDK1 activity (**Fig. 5a**), suggesting Aβ peptide–induced increases in PDK1 activity depend on PrP^C. In $TgA\beta^{pos}$ cultured hippocampal neurons, the amount of TNFR1 at the cell surface was increased by approximately twofold (**Supplementary Fig. 6a**), and the concentration of sTNFR1 in the culture medium was decreased by approximately 50% (**Supplementary Fig. 6b**), as compared to $TgA\beta^{neg}$ neurons. In the culture medium of $TgA\beta^{pos}$ neurons, the concentration of sAPPα was reduced by 50%, whereas the concentrations of sAPPβ, $A\beta_{40}$ and $A\beta_{42}$ were increased by 50–100%, as compared to $TgA\beta^{neg}$ neurons (**Fig. 5b**). As in prion-infected neurons, in $TgA\beta^{pos}$ neurons TACE was enriched in Cav-1–positive vesicles, whereas in $TgA\beta^{neg}$ neurons it was enriched in the plasma membrane (that is, FAK-positive fractions) (**Supplementary Fig. 6c**). Phosphorylation of TACE at residue Thr735 was increased by 2.5-fold in $TgA\beta^{pos}$ neurons as compared to $TgA\beta^{neg}$ neurons (**Fig. 5c**). In $TgA\beta^{pos}$ neurons, inhibition of PDK1 with BX912 decreased TACE phosphorylation (**Fig. 5c**) and promoted its trafficking to the plasma membrane (**Supplementary Fig. 6c**). PDK1 inhibition with BX912 or silencing with PDK1-directed siRNA in $TgA\beta^{pos}$ neurons increased the concentrations of sTNFR1 and sAPPα and decreased the concentrations of sAPPβ, $A\beta_{40}$ and $A\beta_{42}$ in the culture medium

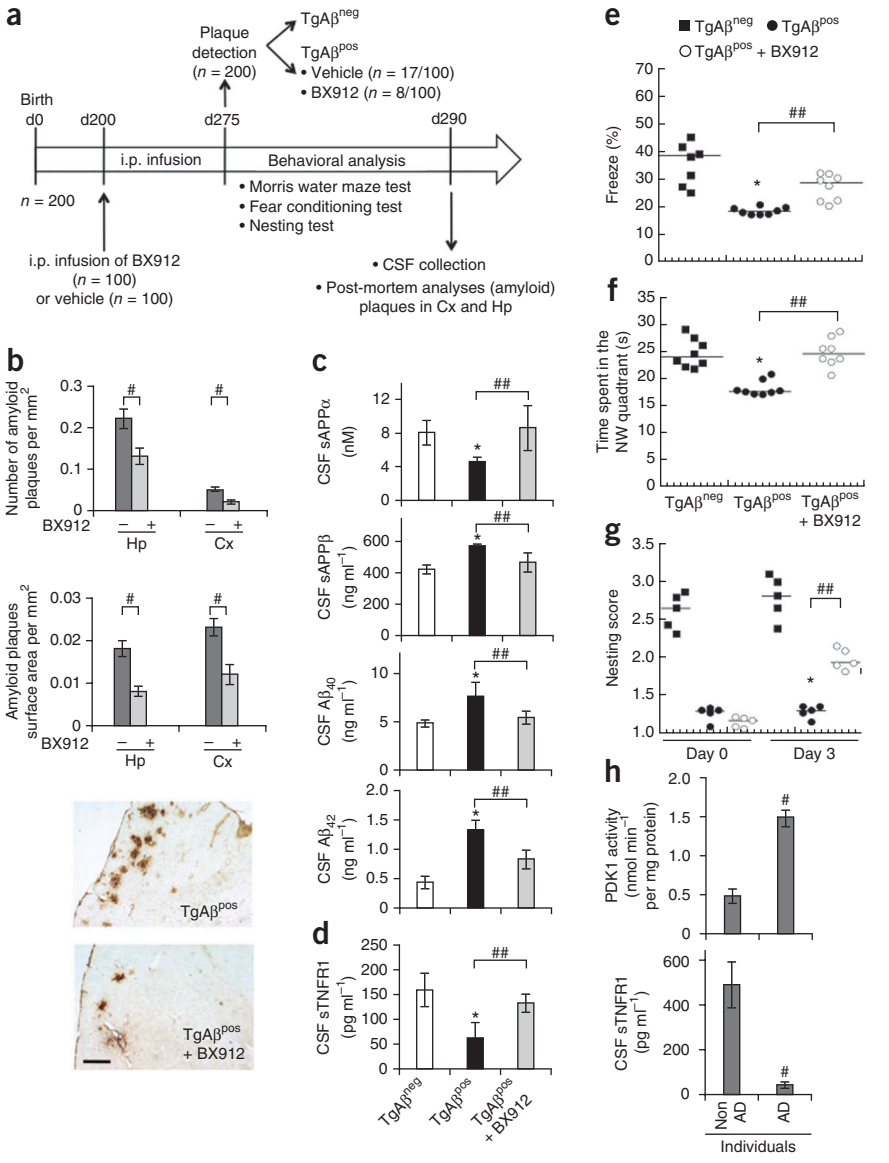

Figure 6 PDK1 inhibition reduces Alzheimer's disease–like pathology and cognitive and memory impairments in Tg2576 mice. (**a**) Schematic of the experimental procedure with Tg2576 mice. (**b**) Number (top) and surface area (middle) of amyloid plaques in the hippocampus (Hp) and cortex (Cx) of TgAβ^{pos} mice treated or not with BX912 ($n = 8$). Values are means ± s.e.m. #$P < 0.001$ versus untreated TgAβ^{pos} mice ($n = 17$). Bottom, representative images of 4G8-positive Aβ plaques in the cortex of TgAβ^{pos} mice treated or not with BX912. Scale bar, 150 μm. (**c**,**d**) Concentration of sAPPα, sAPPβ, $Aβ_{40}$ and $Aβ_{42}$ (**c**) and sTNFR1 (**d**) in the CSF of TgAβ^{pos} mice infused with BX912 as compared to untreated TgAβ^{pos} and TgAβ^{neg} mice ($n = 4$ for each group). Values are means ± s.e.m. *$P < 0.01$ versus TgAβ^{neg} mice; ##$P < 0.01$ versus untreated TgAβ^{pos} mice. (**e**–**g**) Percentage time frozen recorded in the 5-min test trial (% freeze) of the contextual fear conditioning task (**e**), Morris water maze test (**f**) and nest construction (**g**) to assess the impact of BX912-mediated PDK1 inhibition (TgAβ^{pos} + BX912) on Alzheimer's disease–associated memory impairment, as compared to untreated TgAβ^{pos} and TgAβ^{neg} mice. For each group, individual values and median (line) are shown. *$P < 0.01$ versus TgAβ^{neg} mice; ##$P < 0.01$ versus untreated TgAβ^{pos} mice. NW, northwest. (**h**) PDK1 activity in the brain and the concentration of sTNFR1 in the CSF of individuals with Alzheimer's disease ($n = 6$). Values are means ± s.e.m. #$P < 0.01$ versus subjects without Alzheimer's disease.

(**Fig. 5b** and **Supplementary Fig. 6b**). Increased α-secretase–mediated APP processing depends on TACE, as TACE inhibition with TAPI-2 inhibited the effects of BX912 on release of sAPPα, sAPPβ, $Aβ_{40}$ and $Aβ_{42}$ (**Fig. 5b**). Finally, siRNA-mediated silencing of PrP^C in TgAβ^{pos} neurons triggered effects similar to those obtained upon inhibition or silencing of PDK1, which suggests PrP^C may have a dominant role in reducing TACE activity (**Fig. 5b**,**c**). Inhibition of ERK1/2 activity with PD98059 in TgAβ^{pos} neurons did not induce trafficking of TACE to the plasma membrane (**Supplementary Fig. 6c**).

PDK1 inhibition attenuates Alzheimer's disease–like pathology

We next investigated whether inhibition of PDK1 would increase TACE-mediated α-secretase processing of APP in Tg2576 mice and improve memory and cognitive impairments following the experimental schedule described in **Figure 6a**. Injection of BX912 i.p. into 200-day-old Tg2576 mice reduced the number of mice with amyloid plaque deposits at 275 d (BX912-treated TgAβ^{pos} mice) to 8 of 100, as compared to 17 of 100 untreated TgAβ^{pos} mice. The eight BX912-treated TgAβ^{pos} mice had reduced numbers of amyloid plaques and reduced total surface area occupied by plaques in both the hippocampus and cortex as compared to untreated TgAβ^{pos} mice (**Fig. 6b**). The concentrations of sAPPβ, $Aβ_{40}$ and $Aβ_{42}$ decreased in the CSF of BX912-treated TgAβ^{pos} mice and were associated with increased concentration of sAPPα in the CSF as compared to untreated TgAβ^{pos} mice (**Fig. 6c**). The effects on amyloid pathology after BX912 treatment persisted until 330 d, after which BX912-treated TgAβ^{pos} mice were killed (**Supplementary Fig. 7**), indicating that PDK1 inhibition in Tg2576 mice stably increases TACE-mediated α-secretase processing of APP and reduces Aβ production. Furthermore, PDK1 inhibition increased TNFR1 shedding, as we measured an approximately 200% increase in the concentration of sTNFR1 in the CSF of BX912-treated TgAβ^{pos} mice as compared to untreated TgAβ^{pos} mice (**Fig. 6d**). Nevertheless, BX912-treated Tg2576 mice started dying at 350 d because of BX912 toxicity[24], thus limiting the beneficial effect of PDK1 inhibition in transgenic Alzheimer's disease mice.

Finally, BX912 treatment reduced memory and cognitive impairment in Tg2576 mice. PDK1 inhibition with BX912 improved performance in a contextual fear conditioning task, as the percentage of time frozen recorded in BX912-treated 275-day-old TgAβ^{pos} mice was 50% longer as compared to that of untreated 275-day-old TgAβ^{pos} mice (**Fig. 6e**). siRNA-mediated silencing of PDK1 in 275-day-old TgAβ^{pos} mice for 7 d also improved performance in the contextual fear conditioning task (**Supplementary Fig. 8**). BX912 treatment

improved performance in the Morris water maze test, as the time spent in the northwest quadrant by BX912-treated TgAβ^{pos} mice was 50% longer as compared to that of untreated 275-day-old TgAβ^{pos} mice (**Fig. 6f** and **Supplementary Fig. 9**). Nest construction, an affiliative social behavior that is progressively impaired in Tg2576 mice[31], was also partially, but significantly, increased in BX912-treated TgAβ^{pos} mice (**Fig. 6g**). Notably, the beneficial effects on APP processing and memory impairment afforded by PDK1 inhibition with BX912 in Tg2576 mice were also seen in two other mouse models of Alzheimer's disease, 3xTg-AD (ref. 32) and 5xTg-AD (ref. 33) mice (**Supplementary Figs. 10** and **11**). The therapeutic relevance of targeting PDK1 in Alzheimer's disease is substantiated by an approximately 200% increase in PDK1 activity in human Alzheimer's disease whole brains and a 90% decrease in the concentration of sTNFR1 in the CSF of those individuals as compared to age-matched subjects without Alzheimer's disease (**Fig. 6h**).

DISCUSSION

Our findings suggest that PDK1 activity is increased in neurons infected with prions or affected by Aβ deposition. PDK1 inhibition lengthens the survival of PrP^{Sc}-infected mice and mitigates brain pathology and memory impairment in mouse models of Alzheimer's disease.

Our data suggest that PDK1 activation is under the control of PrP^{C} signaling. PrP^{C} positively controls Src kinase and PI3K activities[21,34]. Interestingly, Src kinase–PI3K signaling increases PDK1 activity[22]. PrP^{Sc} may be neurotoxic by stimulating PrP^{C}-associated signaling molecules[35,36], including Src kinases[23,37]. Inhibition of Src kinases, PI3K or PDK1 restores TACE-mediated α-secretase activity at the plasma membrane of infected cells. Thus, chronic recruitment of PrP^{C}-coupled Src kinases and PI3K by PrP^{Sc} may promote increased PDK1 activity in infected neurons.

In Alzheimer's disease, Aβ peptides appear to bind PrP^{C} (refs. 26,27) and upon binding would increase PDK1 activity by promoting recruitment of PrP^{C}-coupled Src kinases and PI3K[38,39]. In agreement with this, PDK1 activity in neurons with amyloid pathology returns to basal levels upon PrP^{C} silencing.

Increased PDK1 activity decreases TACE-mediated α-secretase processing of three major substrates involved in prion or Alzheimer neuropathogeneses, that is, PrP^{C} (ref. 40), APP[2] and TNFR1 (refs. 41,42) (**Supplementary Fig. 12**). This results in the accumulation of PrP^{Sc} in prion disease, increased production of neurotoxic Aβ peptides in Alzheimer's disease, and the enrichment of the plasma membrane with TNFR1 in both pathologies. PDK1 activation in prion-infected or Alzheimer's disease neurons promotes phosphorylation and Cav-1–mediated internalization of TACE, which in turn reduces TACE sheddase activity at the cell surface. PDK1 inhibition is sufficient to rescue TACE-mediated α-secretase activity and to exert beneficial effects in prion and Alzheimer's diseases (**Supplementary Fig. 12**). Indeed, at the plasma membrane of BX912-treated prion-infected cells, TACE catalyzes the α-secretase cleavage of PrP^{C} (ref. 9) into an N-terminally truncated PrP^{C} fragment that cannot convert into PrP^{Sc} and exerts a dominant-negative effect toward prion replication[6]. This mechanism may account for the decreased amount of brain PrP^{Sc}, the increased survival and the improved motor function in 22L-infected mice upon PDK1 inhibition.

In hippocampal neurons from mice with amyloid pathology, PDK1 inhibition increases TACE-mediated α-secretase processing of APP and release of the neuroprotective sAPPα fragment[4,5]. This results in decreased production of $A\beta_{40}$ and $A\beta_{42}$, reduced plaque load in transgenic mice and improved performance in cognitive and memory tasks. Increased amount of TNFR1 in the plasma membrane of prion-infected or Alzheimer's disease neurons is consistent with prior reports describing high expression of TNFR1 (observed by immunolabeling) in the brains of subjects with Alzheimer's disease[41] and prion-infected mice (**Supplementary Fig. 3**). Increased cleavage of TNFR1 and release of soluble TNFR1 upon PDK1 inhibition may reduce prion and Alzheimer's disease neurons from TNF-α–associated inflammatory damage arising from activated microglia[43,44], systemic inflammation[45,46] or aging[47] in prion and Alzheimer's disease. Thus, PDK1 may be targeted in prion and Alzheimer's disease to rescue α-secretase–mediated processing of PrP^{c} and APP.

METHODS

Methods and any associated references are available in the online version of the paper.

Note: Any Supplementary Information and Source Data files are available in the online version of the paper.

ACKNOWLEDGMENTS

We thank G. Bombarde, V. Mutel, F. d'Agostini, G. Zürcher, E. Borroni, J.G. Richards, Z. Lam, M. Bühler, N. Pierron and R. Hochköppler for skillful methodological assistance, C. Vidal for stereotaxic injection of prion strains in mice cerebella, H. Laude and V. Beringue for the use of P3 facilities and F. Brouillard for two-dimensional gel electrophoresis advice. We acknowledge S. Blanquet, M. Briley and A. Baudry for helpful discussions and critical reading of the manuscript. This work was supported by the French Agence Nationale pour la Recherche (Prions&SensiTNF, 1312 01) and INSERM. M.P. is a postdoctoral fellow of French Agence Nationale pour la Recherche. A.A.B. is funded by Domaine d'Intérêt Majeur - Maladies Infectieuses - Région Ile-de-France.

AUTHOR CONTRIBUTIONS

M.P., J.-M.L., O.K. and B.S. conceptualized the study. M.P., C.D., Y.B., J.-M.P., S.H., A.A.-B., J.H.-R., A.R., S.M.-R., S.H. and B.S. performed experiments, and all authors participated in designing experiments and in analyzing and interpreting data. M.P., O.K. and B.S. wrote the manuscript. J.M.L. and B.S. supervised the project.

COMPETING FINANCIAL INTERESTS

The authors declare no competing financial interests.

1. Aguzzi, A., Baumann, F. & Bremer, J. The prion's elusive reason for being. *Annu. Rev. Neurosci.* **31**, 439–477 (2008).
2. Zhang, H., Ma, Q., Zhang, Y.W. & Xu, H. Proteolytic processing of Alzheimer's β-amyloid precursor protein. *J. Neurochem.* **120** (suppl. 1), 9–21 (2012).
3. De Strooper, B., Vassar, R. & Golde, T. The secretases: enzymes with therapeutic potential in Alzheimer disease. *Nat. Rev. Neurol.* **6**, 99–107 (2010).
4. Barger, S.W. & Harmon, A.D. Microglial activation by Alzheimer amyloid precursor protein and modulation by apolipoprotein E. *Nature* **388**, 878–881 (1997).
5. Meziane, H. *et al.* Memory-enhancing effects of secreted forms of the β-amyloid precursor protein in normal and amnestic mice. *Proc. Natl. Acad. Sci. USA* **95**, 12683–12688 (1998).
6. Westergard, L., Turnbaugh, J.A. & Harris, D.A. A naturally occurring, C-terminal fragment of the prion protein delays disease and acts as a dominant negative inhibitor of PrPSc formation. *J. Biol. Chem.* **286**, 44234–44242 (2011).
7. Edwards, D.R., Handsley, M.M. & Pennington, C.J. The ADAM metalloproteinases. *Mol. Aspects Med.* **29**, 258–289 (2008).
8. Gooz, M. ADAM-17: the enzyme that does it all. *Crit. Rev. Biochem. Mol. Biol.* **45**, 146–169 (2010).
9. Vincent, B. *et al.* The disintegrins ADAM10 and TACE contribute to the constitutive and phorbol ester-regulated normal cleavage of the cellular prion protein. *J. Biol. Chem.* **276**, 37743–37746 (2001).
10. Buxbaum, J.D. *et al.* Evidence that tumor necrosis factor α converting enzyme is involved in regulated α-secretase cleavage of the Alzheimer amyloid protein precursor. *J. Biol. Chem.* **273**, 27765–27767 (1998).
11. Sennvik, K. *et al.* Levels of α- and β-secretase cleaved amyloid precursor protein in the cerebrospinal fluid of Alzheimer's disease patients. *Neurosci. Lett.* **278**, 169–172 (2000).

12. Yadavalli, R. *et al.* Calpain-dependent endoproteolytic cleavage of PrPSc modulates scrapie prion propagation. *J. Biol. Chem.* **279**, 21948–21956 (2004).
13. Adrain, C., Zettl, M., Christova, Y., Taylor, N. & Freeman, M. Tumor necrosis factor signaling requires iRhom2 to promote trafficking and activation of TACE. *Science* **335**, 225–228 (2012).
14. D'Alessio, A. *et al.* Plasma membrane microdomains regulate TACE-dependent TNFR1 shedding in human endothelial cells. *J. Cell Mol. Med.* **16**, 627–636 (2012).
15. Wang, Y., Herrera, A.H., Li, Y., Belani, K.K. & Walcheck, B. Regulation of mature ADAM17 by redox agents for L-selectin shedding. *J. Immunol.* **182**, 2449–2457 (2009).
16. Pradines, E. *et al.* Cellular prion protein coupling to TACE-dependent TNF-α shedding controls neurotransmitter catabolism in neuronal cells. *J. Neurochem.* **110**, 912–923 (2009).
17. Mouillet-Richard, S. *et al.* Regulation by neurotransmitter receptors of serotonergic or catecholaminergic neuronal cell differentiation. *J. Biol. Chem.* **275**, 9186–9192 (2000).
18. Mouillet-Richard, S. *et al.* Prions impair bioaminergic functions through serotonin- or catecholamine-derived neurotoxins in neuronal cells. *J. Biol. Chem.* **283**, 23782–23790 (2008).
19. Cronier, S., Beringue, V., Bellon, A., Peyrin, J.M. & Laude, H. Prion strain- and species-dependent effects of antiprion molecules in primary neuronal cultures. *J. Virol.* **81**, 13794–13800 (2007).
20. MacEwan, D.J. TNF receptor subtype signalling: differences and cellular consequences. *Cell Signal.* **14**, 477–492 (2002).
21. Mouillet-Richard, S. *et al.* Signal transduction through prion protein. *Science* **289**, 1925–1928 (2000).
22. Zhang, Q. *et al.* Phosphorylation of TNF-α converting enzyme by gastrin-releasing peptide induces amphiregulin release and EGF receptor activation. *Proc. Natl. Acad. Sci. USA* **103**, 6901–6906 (2006).
23. Pradines, E. *et al.* Pathogenic prions deviate PrP^C signaling in neuronal cells and impair A-β clearance. *Cell Death Dis.* **4**, e456 (2013).
24. Kloo, B. *et al.* Critical role of PI3K signaling for NF-κB–dependent survival in a subset of activated B-cell-like diffuse large B-cell lymphoma cells. *Proc. Natl. Acad. Sci. USA* **108**, 272–277 (2011).
25. Allinson, T.M., Parkin, E.T., Turner, A.J. & Hooper, N.M. ADAMs family members as amyloid precursor protein α-secretases. *J. Neurosci. Res.* **74**, 342–352 (2003).
26. Laurén, J., Gimbel, D.A., Nygaard, H.B., Gilbert, J.W. & Strittmatter, S.M. Cellular prion protein mediates impairment of synaptic plasticity by amyloid-β oligomers. *Nature* **457**, 1128–1132 (2009).
27. Benilova, I. & De Strooper, B. Prion protein in Alzheimer's pathogenesis: a hot and controversial issue. *EMBO Mol. Med.* **2**, 289–290 (2010).
28. Hsiao, K. *et al.* Correlative memory deficits, Aβ elevation, and amyloid plaques in transgenic mice. *Science* **274**, 99–102 (1996).
29. Kawarabayashi, T. *et al.* Age-dependent changes in brain, CSF, and plasma amyloid β protein in the Tg2576 transgenic mouse model of Alzheimer's disease. *J. Neurosci.* **21**, 372–381 (2001).
30. Manook, A. *et al.* Small-animal PET imaging of amyloid-β plaques with [11C]PiB and its multi-modal validation in an APP/PS1 mouse model of Alzheimer's disease. *PLoS ONE* **7**, e31310 (2012).
31. Wesson, D.W. & Wilson, D.A. Age and gene overexpression interact to abolish nesting behavior in Tg2576 amyloid precursor protein (APP) mice. *Behav. Brain Res.* **216**, 408–413 (2011).
32. Oddo, S. *et al.* Triple-transgenic model of Alzheimer's disease with plaques and tangles: intracellular Aβ and synaptic dysfunction. *Neuron* **39**, 409–421 (2003).
33. Oakley, H. *et al.* Intraneuronal β-amyloid aggregates, neurodegeneration, and neuron loss in transgenic mice with five familial Alzheimer's disease mutations: potential factors in amyloid plaque formation. *J. Neurosci.* **26**, 10129–10140 (2006).
34. Santuccione, A., Sytnyk, V., Leshchyns'ka, I. & Schachner, M. Prion protein recruits its neuronal receptor NCAM to lipid rafts to activate p59fyn and to enhance neurite outgrowth. *J. Cell Biol.* **169**, 341–354 (2005).
35. Winklhofer, K.F., Tatzelt, J. & Haass, C. The two faces of protein misfolding: gain- and loss-of-function in neurodegenerative diseases. *EMBO J.* **27**, 336–349 (2008).
36. Pietri, M. *et al.* Overstimulation of PrPC signaling pathways by prion peptide 106–126 causes oxidative injury of bioaminergic neuronal cells. *J. Biol. Chem.* **281**, 28470–28479 (2006).
37. Nixon, R.R. Prion-associated increases in Src-family kinases. *J. Biol. Chem.* **280**, 2455–2462 (2005).
38. Um, J.W. *et al.* Alzheimer amyloid-β oligomer bound to postsynaptic prion protein activates Fyn to impair neurons. *Nat. Neurosci.* **15**, 1227–1235 (2012).
39. Larson, M. *et al.* The complex PrP^C-Fyn couples human oligomeric Aβ with pathological tau changes in Alzheimer's disease. *J. Neurosci.* **32**, 16857–16871 (2012).
40. Mallucci, G. *et al.* Depleting neuronal PrP in prion infection prevents disease and reverses spongiosis. *Science* **302**, 871–874 (2003).
41. Li, R. *et al.* Tumor necrosis factor death receptor signaling cascade is required for amyloid-β protein–induced neuron death. *J. Neurosci.* **24**, 1760–1771 (2004).
42. He, P. *et al.* Deletion of tumor necrosis factor death receptor inhibits amyloid β generation and prevents learning and memory deficits in Alzheimer's mice. *J. Cell Biol.* **178**, 829–841 (2007).
43. Williams, A., Van Dam, A.M., Ritchie, D., Eikelenboom, P. & Fraser, H. Immunocytochemical appearance of cytokines, prostaglandin E_2 and lipocortin-1 in the CNS during the incubation period of murine scrapie correlates with progressive PrP accumulations. *Brain Res.* **754**, 171–180 (1997).
44. Mehlhorn, G., Hollborn, M. & Schliebs, R. Induction of cytokines in glial cells surrounding cortical β-amyloid plaques in transgenic Tg2576 mice with Alzheimer pathology. *Int. J. Dev. Neurosci.* **18**, 423–431 (2000).
45. Perry, V.H. The influence of systemic inflammation on inflammation in the brain: implications for chronic neurodegenerative disease. *Brain Behav. Immun.* **18**, 407–413 (2004).
46. Holmes, C. *et al.* Systemic inflammation and disease progression in Alzheimer disease. *Neurology* **73**, 768–774 (2009).
47. Singh, T. & Newman, A.B. Inflammatory markers in population studies of aging. *Ageing Res. Rev.* **10**, 319–329 (2011).

ONLINE METHODS

Antibodies. The mouse monoclonal antibodies SAF32 (A03202), SAF61 (A03205) and SAF83 (A03207) (SPI-Bio, Montigny-le-Bretonneux, France) were used to detect PrP. The rabbit polyclonal antibody to TNFR1 (JM-3125) was from MBL International (Woburn, MA, USA). Rabbit polyclonal antibodies to TACE (1131) and active caspase-3 (3015) were purchased from QED Bioscience (San Diego, CA, USA) and Biovision (Mountain View, CA, USA), respectively. The rabbit polyclonal antibody to MAP2 (AB5622) was from EMD Millipore (Darmstadt, Germany). The mouse monoclonal antibody to actin (NB600-535) was from Novus Biologicals (Littleton, CO, USA). Rabbit polyclonal antibodies to caveolin-1 (Cav-1) (610059) and focal adhesion kinase (FAK) (sc-932) were obtained from Transduction Laboratories (Lexington, KY, USA) and Santa Cruz Biotechnology (SantaCruz, CA, USA), respectively. Specific rabbit antibody to phosphothreonine (71-8200) was from Zymed Laboratories (San Francisco, CA, USA). Mouse monoclonal antibody to β-amyloid (4G8) (SIG-39220) was from Covance (Princeton, NJ, USA). When nonspecified, primary antibodies were used at 0.5 μg ml^{-1} for western blot experiments and at 5 μg ml^{-1} for immunofluorescence experiments.

Human Alzheimer's disease samples. CSF and frozen post-mortem temporal cortex samples were obtained from six patients and six age- and sex-matched controls (**Supplementary Table 2**) enrolled in a research project approved by the Ethics Committee of Bichat University Hospital (Paris, France). All patients or caregivers gave their written informed consent for CSF assessment and for using post-mortem tissues. The post-mortem intervals (PMIs) never exceeded 24 h. All these patients had an history of progressive dementia. Diagnoses were established by a multidisciplinary team of neurologists and neuropsychologists specialized in cognitive disorders. Diagnosis of Alzheimer's disease was made according to the National Institute of Neurological and Communicative Disorders and Stroke-Alzheimer's Disease and Related Disorders Association (NINCDS-ADRDA) criteria[48]. Age-matched controls had no history of progressive dementia. They were dyspneic, gave informed consent and were recruited from the emergency and internal medicine departments of Lariboisière hospital (Paris, France).

Mice. Adult C57Bl/6J mice were bred and underwent experiments in level-3 biological risk containment, respecting European guidelines for the care and ethical use of laboratory animals (Directive 2010/63/EU of the European Parliament and of the Council of 22 September 2010 on the protection of animals used for scientific purposes). Mice were inoculated with the mouse-adapted 6PB1 bovine spongiform encephalopathy strain or with the cerebellotropic 22L scrapie strain[49] (CNRS Strasbourg, France). 200 Tg2576 (ref. 28) or 3xTg-AD[32] or 5xTg-AD[33] mice of both sexes (all from Hoffmann LaRoche, Basel, Switzerland) were used as models of Alzheimer's disease. CSF was collected from the cisterna magna under anesthesia with 3% isoflurane. All animal procedures were approved by the Comité Régional d'Ethique en Matière d'Expérimentation Animale de Strasbourg (France) and the Animal Care and Use Committee at Basel University (Switzerland).

Chronic intraperitoneal injection of BX912 into mice. Mice were fasted overnight but allowed water *ad libitum* before the experiment. They were then anesthetized with isoflurane inhalation, and a midline incision was performed to insert into the peritoneum the polyethylene catheter of an osmotic pump (Alzet, Cupertino, CA, USA). BX912 or vehicle (1% DMSO in sterile normal saline buffer) was administered at a flow rate of 0.25 μL per h, which corresponded to 100 μg per mouse per day (5 mg kg^{-1} per day). Pumps were replaced every 4 weeks.

***In vivo* siRNA-mediated silencing.** To decrease PDK1 expression *in vivo*, 2 μg of siRNA directed against PDK1 (1 μg μl^{-1}) was injected into the third ventricle three times at 36-h intervals[50] 7 d before behavioral and biochemical analyses. We considered that PDK1 was efficiently silenced when PDK1 activity measured in brain extracts of siRNA-injected mice was reduced by more than 60% as compared to that of siScr-injected mice.

Behavioral testing. Motor function in 22L-infected mice was assessed by the static rod test[51]. For Alzheimer's disease mouse models, contextual fear conditioning[52], Morris water maze task[52] and nest building[31] tests were performed as previously reported.

Cell culture and prion infection. 1C11 cells chronically infected or not by the mouse-adapted 22L or Fukuoka (Fk) strains[18] were grown and induced to differentiate along the serotonergic (1C11$^{5\text{-HT}}$) pathway[17]. Primary CGNs were isolated from dissociated cerebella of 4- to 5-day-old C57Bl/6J mice and infected by the 22L/Fk strains[19].

Isolation and culture of Alzheimer's disease neurons. Cultures of adult hippocampal AD neurons were established from Tg2576 mice as previously reported[53].

Cell viability assays. The viability of ~1 × 10^5 infected or uninfected 1C11 or 1C11$^{5\text{-HT}}$ cells exposed to recombinant mouse sTNF-α (Biosource International, Camarillo, CA, USA) was evaluated by the cellular reduction of 3-(4,5-dimethylthiazol-2-yl)-2,5-diphenyltetrazolium bromide (MTT, Invitrogen, Carlsbad, CA, USA)[36]. Neuronal dysfunction in 22L-infected and uninfected CGNs was evaluated by sTNF-α–induced dendritic fragmentation. CGNs seeded (5.10^5 cells per well) in 12-well plates coated with poly-D-lysine (Sigma-Aldrich, St. Louis, MO, USA) were exposed to sTNF-α. Cells were then fixed and stained with an anti-MAP2 antibody. After imaging with a fluorescence microscope (Zeiss Leica), cells showing fragmented versus nonfragmented dendrites were counted using ImageJ software. Investigators were blinded to treatment conditions.

Immunofluorescent labeling. Immunofluorescent labeling of PrP^C, TNFR1, TACE and MAP2 was performed using standard protocols as reported in refs. 19 and 54. Immunolabeling was analyzed using a Leica DMI6000 B microscope (Wetzlar, Germany) and subjected to image analysis with AQUA software[55].

Cell extract preparation, PNGase assay and western blot analyses. Cells were washed in PBS/Ca^{2+}/Mg^{2+} and incubated for 30 min at 4 °C in lysis buffer (50 mM Tris-HCl pH 7.4, 150 mM NaCl, 5 mM EDTA, 1% Triton X-100, 1 mM Na_3VO_4 and protease inhibitors (Roche)). After centrifugation of the lysate (14,000*g*, 15 min), the protein concentration in the supernatant was measured with the bicinchoninic acid method (Pierce, Rockford, IL, USA). For the PNGase assay, protein extracts were incubated with 500 U N-glycosidase F (PNGase, New England Biolabs, Ipswich, MA, USA) for 1 h at room temperature. Solubilized proteins (20 μg) were resolved by 10% SDS-PAGE. After transfer, blocked membranes were incubated with 0.5 μg ml^{-1} SAF61 primary antibody. Bound antibodies were revealed by enhanced chemiluminescence detection (ECL, Amersham Pharmacia Biotech, Piscataway, NJ, USA). To standardize the results, membranes were rehybridized with an anti-actin antibody. The ratio between the truncated form of PrP (C1 fragment) and full-length PrP (Native)[56] was evaluated by densitometric analyses using ImageJ software.

Soluble TNF-α receptor type 1 quantification. The amount of sTNFR1 was measured in cell culture medium or CSF by ELISA using the Mouse/Rat TNF RI/TNFRSF1A Quantikine ELISA Kit (MRT10) according to the manufacturer's instructions (R&D System, Minneapolis, MN, USA).

TNFR1 expression and PrP^{Sc} deposition in the brains of prion-infected mice. Prion-infected (n = 3 6PB1-inoculated and n = 3 22L-inoculated) and control uninfected (n = 6) mice were killed at 90 (6PB1) and 130 (22L) d after infection by cervical dislocation. Brains were removed and immersed for 24 h in Carnoy's fixative before being dehydrated and embedded in paraffin. Transverse sections (7 μm thick) were cut, and immunoperoxidase staining protocols were used for the detection of PrP^{Sc} and TNFR1 using SAF32 (1 μg ml^{-1}) and anti-TNFR1 (2 μg ml^{-1}) antibodies, respectively[49,57,58]. The specificity of PrP^{Sc} immunodetection was achieved by denaturing the PrP^C by incubation of the sections in proteinase K (10 μg ml^{-1}) for 10 min at 37 °C and subsequently in 3.4 M guanidine thiocyanate for 15 min. The PrP- and TNFR1-bound antibodies were visualized using HRP-conjugated anti-mouse or anti-rabbit immunoglobulins (SouthernBiotech, Birmingham, AL, USA), respectively, and the Vectastain ABC kit (Vector Labs, Burlingame, CA, USA).

doi:10.1038/nm.3302

PrP^C or PDK1 silencing and enzyme inhibition. Cells were transfected with siRNA against PrP^C (refs. 16,36) or PDK1 (target sequence: AACUGGCCACUUCCAGAGAAU) using Lipofectamine 2000 reagent according to the manufacturer's instructions (Invitrogen, Carlsbad, CA, USA).

TACE activity was inhibited with TNF-α processing inhibitor-2 (TAPI-2; Peptides International, Louisville, KY, USA). Src kinase, PI3K, PDK1 and MEK-ERK1/2 kinase activity were inhibited with 4-amino-5-(4-chlorophenyl)-7-(t-butyl)pyrazolo[3,4-d] pyrimidine (PP2) (Calbiochem, San Diego, CA, USA), wortmannin (Calbiochem, San Diego, CA, USA), BX912 (Axon Medchem BV, Groningen, The Netherlands) and PD98059 (Calbiochem, San Diego, CA, USA), respectively.

TACE immunoprecipitation. TACE immunoprecipitation was performed according to standard protocols by using protein A–Sepharose beads (Amersham Pharmacia Biotech, Piscataway, NJ, USA) coupled to anti-TACE antibody and 100 μg of proteins of cell extracts. Immunoprecipitates were analyzed by western blotting using anti-TACE and specific anti-pan phosphothreonine (p-Thr) antibodies as described in ref. 54.

Sucrose gradient fractionation of cell membranes. TACE was detected by western blot analysis after sucrose gradient membrane fractionation of cell extracts performed under detergent-free conditions to isolate low buoyant fractions enriched in caveolin-1 proteins[59]. The cell surface biotinylation assay was performed with EZ-link sulfo-NHS-SS-biotin according to the manufacturer's instructions (Pierce Chemical Co, Rockford, IL, USA). After sucrose gradient fractionation, biotinylated TACE was immunoprecipitated and detected by HRP-conjugated streptavidin. To detect PDK1-dependent TACE translocation back to plasma membrane, infected cells were treated for 1 h with BX912 (1 μM) at 37 °C. Temperature block was performed at 4 °C. TACE was mutated at Thr735 into aspartic acid or alanine and these constructs were transfected using Lipofectamine 2000 (Invitrogen, Carlsbad, CA, USA) into uninfected $1C11^{5\text{-HT}}$ neural cells[60].

Duolink proximity ligation assay. Cells were fixed with 4% paraformaldehyde for 30 min and then washed with PBS. After permeabilization with 0.05% saponin, coverslips were blocked with PBS/3% ovalbumin for 30 min. Immunostaining was performed by simultaneous incubation of anti-TACE and anti–caveolin-1 antibodies. The Duolink proximity ligation assay was subsequently performed by J.M.L. (who was blinded to the treatment conditions) as instructed by the manufacturer (Olink Bioscience, Uppsala, Sweden).

Immunoelectron microscopy. Cells, grown to ~80% confluency, were rinsed twice with PBS, collected in PBS and 10 mM EDTA, and rinsed twice with PBS. The cell pellet was fixed with 0.2% phosphate-buffered glutaraldehyde for 20–120 s and blocked with bovine albumin. Processing of cells for ultrathin cryosectioning and immunolabeling was performed indirectly[61], with 5- or 8-nm gold particles conjugated with affinity-purified goat anti-mouse or anti-rabbit IgG (Invitrogen, Carlsbad, CA, USA)[62]. The labeled specimens were negatively stained with sodium silicotungstate, and images were captured with a JEOL CX100 transmission electron microscope.

Caveolin-1 immunosequestration. Caveolin-1 immunosequestration was performed by cell bombardment with tungsten microprojectiles coated with antibody to Cav-1 (ref. 21).

Two dimensional gel electrophoresis. Two dimensional gel electrophoresis of TACE was performed according to the manufacturer's instructions (Bio-Rad, Hercules, CA, USA) with ~1×10^6 cells.

Measurement of PDK1 activity. PDK1 activity was measured in cell extracts using a fluorescently labeled PDK1 substrate (5FAM-ARKRERTYSFGHHA-COOH, Caliper Life Sciences, Hanover, MD, USA) as reported in ref. 63. The relative amounts of substrate peptide and product phospho-peptide were determined using a Caliper EZ-reader (Caliper Life Sciences, Hanover, MD, USA).

PrP^{res} quantification. The amount of proteinase K–resistant PrP (PrP^{res}) in infected cell extracts or brain extracts of 22L-infected mice treated or not with BX912 were determined using a PrP-specific sandwich ELISA[64] after proteinase K digestion (10 μg ml^{-1}) for 1 h at 37 °C.

Internal granular layer staining. Brains were frozen in dry ice. Parasagittal tissue sections (12 μm) were mounted on slides previously coated with 2% 3-aminopropyl-tri-ethoxysilane in acetone (EGA, Steinheim, Germany) and fixed with 4% paraformaldehyde in PBS, pH 7.4 for 20 min, followed by three 5-min washing steps in PBS. Sections were air dried and stored at −20 °C until use. The sections were immunostained for PCNA[65], and evaluation of viable cells performed with the ^{131}I-labeled staphylococcal protein A (SpA) binding test[66]. Nissl-counterstained sections were examined with bright-field and dark-field optics using a Zeiss Axiophot. The films were used as negatives to produce reverse images, that is, white areas revealing high levels of hybridization signal on a dark background.

***In vivo* amyloid plaque detection.** Amyloid plaques in Tg2576, 3xTg-AD and 5xTg-AD mouse models were detected by PET imaging as reported in ref. 30 using a microPET FOCUS F120 scanner (Siemens Medical Solutions, Bern, Switzerland). The Pittsburgh B compound was from Scintomics (Fuerstenfeldbruck, Germany) and used at a concentration of 1.5 nmol l^{-1}.

Aβ plaque staining and quantification. Tg2576 mice were killed by cervical dislocation at 275 d. Detection of Aβ plaques in the cortex and the hippocampus was performed by using 4G8 antibody (1 μg ml^{-1}) overnight at 4 °C. Tissue sections were next incubated with biotinylated anti-mouse secondary antibody (1 μg ml^{-1}) and incubated for 30 min at room temperature. Then, samples were rinsed and incubated with the Vectastain ABC reagent (Vector Labs, Burlingame, CA, USA) for 30 min. Preparations were then covered with diaminobenzidine at room temperature, gently washed with water, covered with Mayer's hematoxylin, dehydrated with ethanol and xylene and mounted with Super Mount (Innogenex, San Ramon, CA, USA). Samples were analyzed using a Leica DMI6000 B microscope (Wetzlar, Germany) and subjected to image analysis with AQUA software. The number of Aβ plaques was estimated by counting the number of 4G8-positive deposits per slice (expressed as number of Aβ deposits per mm^2). The load of amyloid was estimated by the area stained by 4G8 antibody in relation with the total area analyzed. The investigator was blinded to the treatment conditions.

sAPPα, sAPPβ, $A\beta_{40}$ and $A\beta_{42}$ quantification. The analysis of the different APP cleavage products (sAPPα, sAPPβ, $A\beta_{40}$ and $A\beta_{42}$) was performed using one- and two-dimensional gel electrophoresis, immunoblotting and mass spectrometry[67]. Quantifications were achieved by a stable-isotope dilution methodology in combination with LC-MS/MS[68].

Data analysis. An analysis of variance of the cell/animal response group was performed using Kaleidagraph software (Synergy Software, Reading, PA, USA). Values are given as means ± s.e.m. Significant responses ($P < 0.05$) are marked by symbols (#,*) and their corresponding P values are provided in figure legends. Survival times were analyzed by Kaplan-Meier survival analysis using a log-rank test for curve comparisons.

48. McKhann, G. *et al.* Clinical diagnosis of Alzheimer's disease: report of the NINCDS-ADRDA Work Group under the auspices of Department of Health and Human Services Task Force on Alzheimer's Disease. *Neurology* **34**, 939–944 (1984).
49. Vidal, C. *et al.* Early dnmysfunction of central 5-HT system in a murine model of bovine spongiform encephalopathy. *Neuroscience* **160**, 731–743 (2009).
50. Baudry, A., Mouillet-Richard, S., Schneider, B., Launay, J.M. & Kellermann, O. miR-16 targets the serotonin transporter: a new facet for adaptive responses to antidepressants. *Science* **329**, 1537–1541 (2010).
51. Kempster, S., Bate, C. & Williams, A. Simvastatin treatment prolongs the survival of scrapie-infected mice. *Neuroreport* **18**, 479–482 (2007).
52. Cramer, P.E. *et al.* ApoE-directed therapeutics rapidly clear β-amyloid and reverse deficits in AD mouse models. *Science* **335**, 1503–1506 (2012).
53. Brewer, G.J. & Torricelli, J.R. Isolation and culture of adult neurons and neurospheres. *Nat. Protoc.* **2**, 1490–1498 (2007).
54. Loubet, D. *et al.* Neuritogenesis: the prion protein controls β1 integrin signaling activity. *Faseb J.* **26**, 678–690 (2012).
55. McCabe, A., Dolled-Filhart, M., Camp, R.L. & Rimm, D.L. Automated quantitative analysis (AQUA) of in situ protein expression, antibody concentration, and prognosis. *J. Natl. Cancer Inst.* **97**, 1808–1815 (2005).

56. Mouillet-Richard, S., Laurendeau, I., Vidaud, M., Kellermann, O. & Laplanche, J.L. Prion protein and neuronal differentiation: quantitative analysis of prnp gene expression in a murine inducible neuroectodermal progenitor. *Microbes Infect.* **1**, 969–976 (1999).
57. Bailly, Y. *et al.* Prion protein (PrPc) immunocytochemistry and expression of the green fluorescent protein reporter gene under control of the bovine PrP gene promoter in the mouse brain. *J. Comp. Neurol.* **473**, 244–269 (2004).
58. Heitz, S. *et al.* BAX contributes to Doppel-induced apoptosis of prion-protein–deficient Purkinje cells. *Dev. Neurobiol.* **67**, 670–686 (2007).
59. Song, K.S. *et al.* Co-purification and direct interaction of Ras with caveolin, an integral membrane protein of caveolae microdomains. Detergent-free purification of caveolae microdomains. *J. Biol. Chem.* **271**, 9690–9697 (1996).
60. Soond, S.M., Everson, B., Riches, D.W.H. & Murphy, G. ERK-mediated phosphorylation of Thr735 in TNF-α–converting enzyme and its potential role in TACE protein trafficking. *J. Cell Sci.* **118**, 2371–2380 (2005).
61. Slot, J.W., Geuze, H.J., Gigengack, S., Lienhard, G.E. & James, D.E. Immuno-localization of the insulin regulatable glucose transporter in brown adipose tissue of the rat. *J. Cell Biol.* **113**, 123–135 (1991).
62. Slot, J.W. & Geuze, H.J. A new method of preparing gold probes for multiple-labeling cytochemistry. *Eur. J. Cell Biol.* **38**, 87–93 (1985).
63. Hofler, A. *et al.* Study of the PDK1/AKT signaling pathway using selective PDK1 inhibitors, HCS, and enhanced biochemical assays. *Anal. Biochem.* **414**, 179–186 (2011).
64. Bate, C., Langeveld, J. & Williams, A. Manipulation of PrPres production in scrapie-infected neuroblastoma cells. *J. Neurosci. Methods* **138**, 217–223 (2004).
65. Raucci, F. *et al.* Proliferative activity in the frog brain: a PCNA-immunohistochemistry analysis. *J. Chem. Neuroanat.* **32**, 127–142 (2006).
66. Moss, T.J., Rosenblatt, H.M. & Seeger, R.C. Expression of a developmental stage-specific antigen by neuronal precursor cells of human fetal cerebellum. *J. Neuroimmunol.* **20**, 3–14 (1988).
67. Schieb, H. *et al.* β-amyloid peptide variants in brains and cerebrospinal fluid from amyloid precursor protein (APP) transgenic mice: comparison with human Alzheimer amyloid. *J. Biol. Chem.* **286**, 33747–33758 (2011).
68. Ciccimaro, E. & Blair, I.A. Stable-isotope dilution LC-MS for quantitative biomarker analysis. *Bioanalysis* **2**, 311–341 (2010).

doi:10.1038/nm.3302